# Reacting Turbulent Boundary-Layer Approach to Solid Propellant Erosive Burning

Robert A. Beddini*
*Aeronautical Research Associates of Princeton, Inc., Princeton, N.J.*

**A theoretical analysis of the erosive burning of solid propellants is presented using a reacting turbulent boundary-layer approach. The turbulent field is modeled using the second-order closure technique and a single-step gas-phase reaction is assumed for the combustion of a homogeneous propellant. Calculated results agree with the generally observed erosive burning trends of threshold velocity, nonlinear recession-ratio velocity dependence, pressure dependence, and normal burning-rate sensitivity. For constant external velocity boundary layers, the results show a decrease in burning rate along the propellant surface which has also been experimentally observed. Examination of calculated profiles of mean-temperature and turbulent correlations in the boundary layer reveals that erosive burning is predominantly caused by flame-zone broadening due to the diffusive effects of turbulence.**

## Nomenclature

$A$ = Arrhenius pre-exponential coefficient
$a,b$ = modeling parameters (3.25, 0.125)
$c_p$ = specific heat at constant pressure
$c_\pi$ = specific heat of propellant
$D$ = overall diffusion coefficient
$g_{lm}$ = metric tensor, $\partial x_l/\partial x_m$
$h$ = specific sensible enthalpy
$h_\alpha^0$ = heat of formation at 0 K
$H$ = total enthalpy, $H=h+u^iu_i/2$
$k$ = thermal conductivity
$L_s^0$ = heat of decomposition at 0 K
$\dot{m}_s$ = surface mass flux
$n$ = normal burning-rate pressure-exponent
$n_j$ = surface normal vector
$p$ = hydrostatic pressure
$p_*$ = reference pressure, $6.9\times10^7$ dyn/cm$^2$ (1000 psi)
$q_j$ = heat-transfer vector
$\dot{r}$ = recession (burning) rate, $\dot{m}_s/\rho_\pi$
$\dot{r}_n$ = normal (nonerosive) recession rate
$\dot{r}_*$ = $\dot{r}_n(p_*)$
$R$ = gas constant per unit mole
$s$ = width of two-dimensional channel
$S_\alpha$ = symbol of chemical species $\alpha$
$t$ = time
$T$ = temperature
$T_A$ = activation temperature (energy/$R$)
$T_i$ = interior propellant temperature
$u_j$ = velocity vector $\{u,v,w\}$
$U_e$ = velocity external to boundary layer
$U_e^0$ = $U_e(x=0)$
$\dot{w}_\alpha$ = rate of production of species $\alpha$ per unit mass
$W_\alpha$ = molecular weight of species $\alpha$
$x_j$ = coordinate vector $\{x,y,z\}$
$Y_\alpha$ = mass fraction
$\beta$ = temperature exponent of reaction pre-exponential coefficient
$\Delta h_g$ = heat of reaction per unit mass
$\Lambda$ = turbulent macrolength scale
$\mu$ = viscosity
$\xi$ = length of initial adiabatic surface
$\rho$ = density
$\phi$ = $\sum_\alpha \nu_\alpha'' W_\alpha$
$\Phi$ = concentration (pressure) exponent in reaction rate

*Superscripts*

$\bar{(\ )}$ = time average of variable
$(\ )'$ = turbulent fluctuating value of variable

*Subscripts*

$F$ = fuel
$g$ = gas phase
$e$ = value external to boundary layer
$O$ = oxidizer
$s$ = propellant surface value
$\alpha$ = index for chemical species
$\pi$ = propellant solid phase
0 = stagnation value
, = differentiation

Presented as Paper 77-931 at the AIAA/SAE 13th Propulsion Conference, Orlando, Fla., July 11-13, 1977; submitted Nov. 30, 1977; revision received June 8, 1978. 

Index categories: Solid and Hybrid Rocket Engines; Boundary Layers and Convective Heat Transfer—Turbulent.

*Associate Consultant. Member AIAA.

## Introduction

THE term "erosive burning" refers to the increase in solid propellant burning rate in the presence of a convective flow parallel to the propellant surface. Most current motor designs utilize a central port within the propellant grain through which the combustion gases flow. As the flow velocity increases toward the aft end of the port, a position is reached where the propellant burning rate due to erosion may exceed the normal (strand) burning rate by several percent. This increase must be accurately accounted for in the prediction of overall motor thrust performance. In addition, recent design trends to high-port velocity ($M\approx1$) and nozzleless rocket motors further accentuate the erosion effect.

Literature reviews of erosive burning observations and theoretical treatments have been reported in Williams et al.,[1] King,[2] and Kuo and Razdan.[3] Various mechanisms have been hypothesized to account for erosive burning behavior. For example, the mechanism first proposed by Corner[4] is that the turbulent boundary layer on the surface of the propellant increases the effective thermal diffusivity in the flame zone, thus increasing heat transfer to the propellant. This hypothesis is used in several erosive burning theories, including those of Vandenkerckhove[5] (for homogeneous propellants) and Lengellé[6] (for composite propellants). A substantially different cause of erosive burning was proposed by Lenoir and Robillard.[7] They assumed erosive burning to be caused by increased surface heat transfer from the hot

"core" gas external to the boundary layer and added this effect to the normal burning rate. King has criticized the Lenoir-Robillard theory, noting that strong dependence on core-gas temperature is contradicted by experimental observations. King develops an alternative theory for composite propellant erosive burning which is based on the mechanism of convective bending of the diffusion-controlled flame zone. As the total combustion length scale is assumed constant, the resulting flame zone lies closer to the propellant surface and provides increased heat transfer.

The preceding theories are here termed of integral type and offer the advantage of providing practical solutions for surface recession (burning) rate in algebraic form. However, they have two major deficiencies. If the supposed physical cause of erosive burning is erroneous, the theoretical method constructed upon the cause may be of questionable predictive utility (three different causes have been discussed; others have been proposed in the literature). The second deficiency of integral theories at their present stage of development is their use of greatly simplified descriptions of fluid dynamic profiles in the flame zone. For example, the theories of Lengellé and King use incompressible turbulent-velocity profiles in a region where the gas density is typically changing by a factor of three. The accuracy of the velocity-profile description (whether affected by density or other source) directly affects the results of Lengellé, since the erosive contribution to burning rate is assumed proportional to velocity gradient. The flame-bending model of King is also quite sensitive to velocity profile.

An approach to erosive burning is needed which can account for most hypothesized causes of erosive burning and improve the fluid dynamic descriptions used in contemporary integral theories. Therefore, an analysis of the basic differential equations appropriate for a reacting boundary-layer flow is pursued. This type of analysis has been termed an aerothermochemical approach in the prior laminar-flow studies of Tsuji[8] and Schuyler and Torda.[9] The objectives of the present study are to investigate the role of turbulence in erosive burning and to qualitatively validate the basic approach through comparison with several observed erosive burning trends. The approach accounts for the effects of turbulence on boundary-layer heat, mass, and momentum transfer through use of the semiempirical second-order turbulence-closure technique.[10] A single-step gas-phase reaction is assumed for the combustion of a homogeneous propellant. Although an idealization, this type of reaction mechanism is believed adequate for trend analysis, as reviews of erosive burning experimental observations[1,3] indicate that several trends are common to both homogeneous and composite propellants.

## Analysis

Figure 1 shows the geometry under consideration, which is quite similar to the proposed experimental apparatus of Razdan and Kuo.[11] A boundary layer develops along an adiabatic surface of length $\xi$, and undergoes transition to turbulent flow before encountering the propellant. Due to approximations which will be imposed in this section, the composition and total enthalpy of the initial "driver" flow are taken to be identical to those of the test propellant combustion products. The two-dimensional, symmetric channel through which the combustion gases flow is assumed to be maintained at constant width $s$.

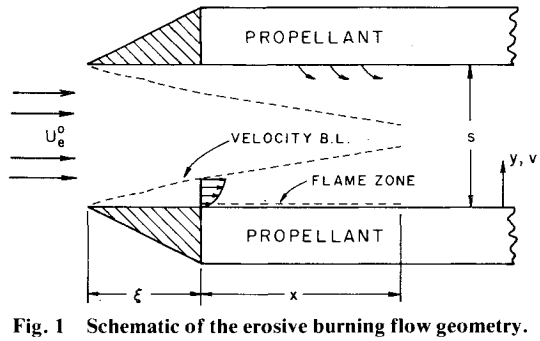


Fig. 1 Schematic of the erosive burning flow geometry.

The fundamental differential equations are adapted from Williams.[12] A single-species diffusion coefficient is assumed, and the effects of thermodiffusion and bulk viscosity are neglected. General tensor notation is used to aid in the manipulations required for turbulence analysis, and to extend the validity of the analysis to axisymmetric flow. Covariant differentiation and differentiation with respect to scalar variables are denoted by a comma. The species index $\alpha$ ranges from 1 through $N$. The equations for conservation of mass, momentum, species mass fraction, total enthalpy, and the equation of state are:

$$\rho_{,t} + (\rho u^{\ell})_{,\ell} = 0 \tag{1}$$

$$\rho(u_{j,t} + u^{\ell} u_{j,\ell}) = -p_{,\ell} + g^{\ell m}[\mu(u_{j,m} + u_{m,j})]_{,\ell} \tag{2}$$

$$(\rho Y_{\alpha})_{,t} + (\rho u^{\ell} Y_{\alpha})_{,\ell} = g^{\ell m}(\rho D Y_{\alpha,m})_{,\ell} + \dot{w}_{\alpha} \tag{3}$$

$$(\rho H)_{,t} + (\rho u^{\ell} H)_{,\ell} = g^{\ell m}\left[kT_{,m} + \rho D \sum_{\alpha} h_{\alpha} Y_{\alpha,m} + \frac{1}{2}\mu(u^{i}u_{i})_{,m}\right]_{,\ell} - \sum_{\alpha} h_{\alpha}^{0} \dot{w}_{\alpha} + p_{,t} + (\mu u^{m} u^{\ell}_{,m})_{,\ell} \tag{4}$$

$$p = \rho R T \sum_{\alpha} Y_{\alpha}/W_{\alpha} \tag{5}$$

For the present analysis, the following assumptions are initially invoked:

Assumption 1: Specific heats of the species are equal and independent of temperature.

Assumption 2: $k/c_p = \rho D = \mu(T)$.

Assumption 3: Combustion of the stoichiometric mixture proceeds through the single-step reaction

$$\sum_{\alpha} \nu'_{\alpha} S_{\alpha} \rightarrow \sum_{\alpha} \nu''_{\alpha} S_{\alpha}$$

where $S_{\alpha}$ are the symbols of the $N$ chemical species, and $\nu'_{\alpha}$ and $\nu''_{\alpha}$ are the stoichiometric coefficients of reactants and products. Specifically considered is the reaction fuel + oxidizer → products, for which the chemical production term is of the form

$$\dot{w}_{\alpha} = (\nu''_{\alpha} - \nu'_{\alpha}) W_{\alpha} \omega$$

with $\omega$ assumed as

$$\omega = A_g T^{\beta g} \exp(-T_{A_g}/T)(\rho Y_F/W_F)^{\Phi_F}(\rho Y_0/W_0)^{\Phi_0}$$

The concentration exponents $\Phi_F$ and $\Phi_0$ have not been restricted to be stoichiometric, as is usually done.[1,8,12] In this way, the concentration exponents may be selected to better approximate the reaction pressure-dependence within the constraint of the single-step reaction.

The immediate objective in using the assumptions is to linearly relate the mass fractions to the total enthalpy. This has been done in the case of normal propellant burning by Johnson and Nachbar,[13] and in the laminar aerothermochemical analysis of Tsuji. To investigate the condition of similarity in turbulent flow, consideration must be given to the boundary conditions at the solid surface and boundary-layer edge in a general coordinate system. This is necessary to provide consistency with the differential equations prior to

Reynolds (time) averaging and the imposition of boundary-layer assumptions.

Following Johnson and Nachbar,[13] reference mass fractions $Y_{\alpha *}$ are defined at the initial state of the reaction such that

$$Y_{\alpha *} = \nu'_\alpha W_\alpha / \phi \tag{6}$$

where

$$\phi = \sum_\alpha \nu'_\alpha W_\alpha = \sum_\alpha \nu''_\alpha W_\alpha$$

The mass fractions at the end state of the reaction (equivalently, external to the boundary layer) are

$$Y_{\alpha e} = \nu''_\alpha W_\alpha / \phi \tag{7}$$

and the propellant-gas interface boundary conditions for $Y_\alpha$ and $H$ are

$$\dot{m}_s (Y_{\alpha s} - Y_{\alpha *}) = \rho D n^j Y_{\alpha,j} |_s \tag{8}$$

$$\dot{m}_s L_s - n^j \dot{q}_{\pi j} = (k/c_p) n^j H_{,j} |_s \tag{9}$$

In the above equations $\dot{m}_s = \rho u_j n^j |_s$ is the surface mass flux, $n^j$ is the unit vector normal to the propellant surface, $L_s$ is the heat of decomposition between the solid and gas states (defined negative for exothermic heat of decomposition), and $\dot{q}_{\pi j}$ is the heat-flux vector out of the propellant. Nonadiabatic processes (e.g., radiation) have been excluded from Eq. (9). If it is assumed at this stage that the heat flux in the propellant is one-dimensional and steady, then

$$-n^j \dot{q}_{\pi j} |_s = n^j \dot{m}_s c_\pi (T_s - T_i)$$

The heat of decomposition is taken to be of the form appropriate for a "perfect" substance[14]

$$L_s = L_s^0 + (c_p - c_\pi) T_s \tag{10}$$

The asymptotic boundary conditions for species and total enthalpy at the edge of the boundary layer are given by Eq. (7) for $Y_\alpha$, and by an overall energy balance for $H$. Defining the heat of reaction (energy/unit mass of product) as

$$\Delta h_g = \phi^{-1} \sum_\alpha (\nu'_\alpha - \nu''_\alpha) W_\alpha h_\alpha^0 = \sum_\alpha (Y_{\alpha *} - Y_{\alpha e}) h_\alpha^0$$

the adiabatic energy balance between the propellant surface and boundary-layer external flow is[8,13]

$$H_e - H_s = \Delta h_g - L_s - c_\pi (T_s - T_i) \tag{11}$$

where $H_e = H_0$ is the constant stagnation enthalpy of the gas. At flow stagnation, the flame temperature is defined as $T_0 = H_0 / c_p$. Equation (11) is independent of $H_s$ in view of Eq. (10).

New dependent variables are defined such that

$$f_\alpha = \phi^{-1} (Y_\alpha - Y_{\alpha *}) / (Y_{\alpha e} - Y_{\alpha *})$$

$$f_H = (H - H_e + \Delta h_g) / (\phi \Delta h_g)$$

Utilizing Assumptions (1-3), the mass fraction and enthalpy equations (3) and (4) may be written as

$$(\rho f_\alpha)_{,t} + (\rho u^\ell f_\alpha)_{,\ell} = g^{\ell m} (\mu f_{\alpha,m})_{,\ell} + \omega \tag{12}$$

$$(\rho f_H)_{,t} + (\rho u^\ell f_H)_{,\ell} = g^{\ell m} (\mu f_{H,m})_{,\ell} + \omega$$
$$+ (\phi \Delta h_g)^{-1} [p_{,t} + (\mu u^m u^\ell_{,m})_{,\ell}] \tag{13}$$

The boundary conditions for $f_\alpha$ and $f_H$ ($=f$, say) may both be written as

$$f = (\dot{m}_s)^{-1} \mu n^j f_{,j} \tag{14}$$

at the surface, and

$$f = 1/\phi \tag{15}$$

at the boundary-layer edge. The following is also assumed:

Assumption 4: The term in brackets in Eq. (13) is negligible for the turbulent boundary-layer flow of interest. This assumption has been discussed in Ref. 15. It is expected to be valid for steady, boundary-layer flows (Assumptions 5 and 6 below) up to low-supersonic conditions. For hypersonic flows, correlations with the fluctuating component of the bracketed term may be significant.[16]

Hence, Eqs. (12) and (13) imply that $f_\alpha = f_H$ throughout the region bounded by Eqs. (14) and (15). This result is important, since it follows a linear relation between both the mean and fluctuating (turbulent) components of $Y_\alpha$ and $H$ in the boundary layer. Specifically, Reynolds averaging yields

$$\bar{Y}_\alpha = Y_{\alpha e} + (Y_{\alpha e} - Y_{\alpha *})(\bar{H} - H_e) / \Delta h_g \tag{16}$$

$$Y'_\alpha = (Y_{\alpha e} - Y_{\alpha *}) H' / \Delta h_g \tag{17}$$

The analysis of turbulence follows the second-order closure approach rather than the use of an eddy diffusivity to model turbulence effects. The reasons for using the second-order approach include the following.

1) Measurements of turbulence in a cold-flow simulation of a grain port have been reported by Yamada, Goto, and Ishikawa.[17] Their results show that while the mean longitudinal-velocity profile apparently achieves similarity, the maximum mean-turbulence value continues to increase in magnitude and moves closer to the port surface with distance from the head end. This nonsimilarity between turbulence and mean velocity precludes consideration of customary formulations of eddy diffusivity.[16]

2) If an eddy diffusivity (or mixing length) formulation is assumed, it would have to include the effects of mass injection, viscous sublayer dissipation, and large streamwise pressure gradient on turbulent transport. These effects are included in the second-order closure approach.

3) The second-order closure approach has been successfully applied to a variety of flows,[10,18,19] and is not empirically particularized for application to erosive burning.

Since application of the turbulence modeling to boundary-layer-type flows is intended, the basic compressible flow equations and numerical solution technique of Sullivan[20] will be modified to accommodate propellant combustion. Sullivan consideres an energy equation for $h = c_p T = H - u^i u_i / 2$, which can be derived by subtracting the equation for kinetic energy from Eq. (4). Therefore, the chemical heat release term in Eq. (4) must be added to the basic enthalpy equation of Sullivan, with the mass fractions related by the present Eqs. (16) and (17). An evaluation of the turbulence modeling for nonreactive flows using the computer code of Sullivan is given by Rubesin et al.[19]

It is now conveient to refer to a Cartesian system with spatial coordinates $\{x,y,z\}$, and velocities $\{u,v,w\}$. Additional assumptions are that:

Assumption 5: The flow is quasi-steady (e.g., $\bar{h}_{,t} = 0$), and two-dimensional ($\partial / \partial z = 0 = \bar{w}$).

Assumption 6: The flow is of boundary-layer type, with outer boundary conditions and static pressure specified by asymptotic matching to an isentropic, one-dimensional flow. This assumption should be adequately satisfied for "driver flow" experimental apparatus (i.e., Ref. 11) in which the channel separation $s$ is relatively large. However, in actual grain ports the acceleration of flow may significantly affect

erosion. To qualitatively assess the acceleration effect, it is further assumed that for finite values of $s$, the velocity at the boundary layer edge is given by

$$U_e(x) = \frac{\rho_e^0 U_e^0}{\rho_e} + \frac{2}{\rho_e s}\int_0^x \dot{m}_s dx$$

with edge density, pressure, and enthalpy determined from isentropic relations upon specifying stagnation values. These relations imply that $U_e$ is assumed equivalent to the bulk velocity in the channel, and that the effects of surface friction and normal injection on stagnation pressure are neglected. A more comprehensive analysis should not only account for the above effects, but also account for the two-dimensional nature of the outer flow as well. The latter effect has been observed in the cold-flow grain-port simulations of Yamada et al.[17] and Dunlap et al.[21]

Assumption 7: Turbulent correlations involving the chemical source term are taken to be zero in the present analysis. This assumption is invoked because complete and consistent models for $\omega'$ correlations are unavailable. Such models are under development by Varma et al.[18] and other investigators. The difficulty in obtaining simple models of the $\omega'$ correlations is predominantly due to the inaccuracy of Taylor expansion of the Arrhenius exponential factor. The potential effect of these correlations is probably not negligible, and they may account for "negative erosion."[22]

#### Final Equations

Under Assumptions 1-7, the final system consists of coupled differential equations for $\bar{u}$, $\bar{v}$ (from mean continuity), $\bar{h}$, $\overline{u'u'}$, $\overline{u'v'}$, $\overline{v'v'}$, $\overline{w'w'}$, $\overline{\rho'u'}$, $\overline{\rho'v'}$, $\overline{h'u'}$, $\overline{h'v'}$, and $\overline{h'h'}$. The second-order correlation equations are quite lengthy and are not listed here. They correspond with the correlation equations of Sullivan but with the terms $\phi\Delta h\overline{\chi'\omega'}$ (where $\chi'$ represents $u'$, $v'$, $2h'$) added to the right-hand sides of the $\overline{h'u'}$, $\overline{h'v'}$, and $\overline{h'h'}$ equations. In accordance with Assumption 7, $\overline{\chi'\omega'}$ is taken to be zero. The mean equations for conservation of mass, momentum, enthalpy, and the equation of state are

$$(\bar{\rho}\bar{u})_{,x} + (\bar{\rho}\bar{v} + \overline{\rho'v'})_{,y} = 0 \tag{18}$$

$$\bar{\rho}\bar{u}\bar{u}_{,x} + (\bar{\rho}\bar{v} + \overline{\rho'v'})\bar{u}_{,y} + (\bar{\rho}\overline{u'v'})_{,y} = -\bar{p}_{,x} + (\bar{\mu}\bar{u}_{,y})_{,y} \tag{19}$$

$$\bar{\rho}\bar{u}\bar{h}_x + (\bar{\rho}\bar{v} + \overline{\rho'v'})\bar{h}_{,y} + (\bar{\rho}\overline{h'v'})_{,y} = \bar{u}\bar{p}_x + \bar{\mu}\left[(\bar{u}_{,y})^2 + \frac{q^2}{\Lambda^2}\left(a + b\frac{\bar{\rho}q\Lambda}{\mu}\right)\right] + (\bar{\mu}\bar{h}_{,y})_{,y} + \phi\Delta h_g\bar{\omega} \tag{20}$$

$$\bar{p} = R\bar{\rho}\bar{T}\left[\sum_\alpha \bar{G}_\alpha(1 - \overline{T'T'}/\bar{T}^2) - \left(\sum_\alpha \overline{G'_\alpha T'}\right)\Big/\bar{T} - \sum_\alpha\sum_\beta (\overline{G'_\alpha G'_\beta})\Big/\sum_\alpha \bar{G}_\alpha\right] \tag{21}$$

In Eq. (21), $G_\alpha = Y_\alpha/W_\alpha$, and the assumption that $|p'|$ is relatively small has been used. Using Eqs. (16) and (17), and Assumption 7, the source term of Assumption 3 may be written as

$$\phi\bar{\omega} = B_g\bar{T}^{\beta_g}\exp(-T_{Ag}/\bar{T})\left[\bar{\rho}\left[\frac{H_e - \bar{H}}{\Delta h_g}\right)\right]^{\Phi_F+\Phi_O}$$

where

$$B_g = \phi A_g(Y_{F_*}/W_F)^{\Phi_F}(Y_{O_*}/W_O)^{\Phi_O}$$

#### Boundary Conditions

The surface boundary conditions for Eqs. (18-20) and the turbulent correlation equations are

$$\bar{v}_s = \dot{\bar{m}}_s/\bar{\rho}_s, \quad \bar{u}_s = 0 \text{ and } \bar{h}_s = c_p\bar{T}_s(\dot{\bar{m}}_s)$$

All correlations are assumed zero at the surface. A linear pyrolysis relation[13]

$$\dot{\bar{m}}_s = A_\pi\bar{T}^{\beta_\pi}\exp(-T_{A\pi}/\bar{T}_s)$$

is used in conjunction with the interface condition [Eq. (9)] to determine $\dot{\bar{m}}_s$ and $\bar{T}_s$.

The asymptotic boundary conditions applied as $y \to \infty$ are:

$$\bar{u} = U_e(x) \text{ and } \bar{h} = h_e(x)$$

All correlations are assumed to be zero in the external stream, with the exception that $\overline{u'u'} = \overline{v'v'} = \overline{w'w'} = 10^{-3}\ (U_e^0)^2$. The parameter $U_e^0 = U_e(x=0)$ is specified by the initial conditions.

#### Initial Conditions

The initial conditions applied at $x=0$ (Fig. 1) are approximately appropriate to an isothermal turbulent boundary layer at a Reynolds number (based on $\xi$, $U_e^0$, $T_0$, and $p_0$) of $10^7$. Near the surface, the temperature profile is faired to avoid prescribing an infinite heat transfer at $x=0^+$. A more complete description of initial profile selection is given in Ref. 15.

**Table 1 Fixed parameters**

| | | | |
|---|---|---|---|
| $T_0$ | $=2900$ K | $T_i$ | $=300$ K |
| $c_p$ | $=0.414$ cal/g-K | $\rho_\pi$ | $=1.62$ g/cm$^3$ |
| $W_\alpha$ | $=W=27.1$ g/g-mole | $\beta_\pi$ | $=0$ |
| $T_{Ag}$ | $=2.0\times10^4$ K | $A_\pi$ | $=1.588\times10^6$ g/cm$^2$-s |
| $L_S^0$ | $=-20$ cal/g | $T_{A\pi}$ | $=1.0\times10^4$ K |
| $\beta_g$ | $=0$ | $c_\pi$ | $=0.35$ cal/g-K |
| $\mu$ | $=0.87\times10^{-6}W^{0.5}T^{0.65}$ | | |

**Table 2 Computational conditions**

| Run | $p_0\times10^{-7}$ dyn/cm$^2$ | $B_g$[a] | $\dot{r}_*$ cm/s | $\Phi_F+\Phi_O$ | $n$ | $U_e^0$, m/s | $s$, cm |
|---|---|---|---|---|---|---|---|
| 1 | 6.897 | $5.94\times10^{11}$ | 0.9383 | .16 | 0.808 | 400 | $\infty$ |
| 2 | | | | | | 100 | 2.0 |
| 3 | | | | | | | 1.0 |
| 4 | | | | | | | 0.7 |
| 5 | | | | | | | 0.5 |
| 6 | | $2.97\times10^{11}$ | 0.6684 | | 0.807 | | 2.0 |
| 7 | | | | | | | 1.0 |
| 8 | | | | | | | 0.7 |
| 9 | | | | | | | 0.5 |
| 10 | | | | | | | $\infty$ |
| 11 | | | | | | 200 | |
| 12 | | | | | | 300 | |
| 13 | | | | | | 400 | |
| 14 | | | | | | 500 | |
| 15 | | | | | | 600 | |
| 16 | | | | | | 700 | |
| 17 | | | | | | 800 | |
| 18 | 10.346 | | | | | 100 | 0.5 |
| 19 | 3.449 | | | | | 100 | 0.5 |
| 20 | 6.987 | $1.19\times10^{12}$ | 1.3387 | | 0.790 | 400 | $\infty$ |
| 21 | | | | | | 100 | 0.7 |
| 22 | | | | | | | 0.5 |
| 26 | 6.897 | $3.95\times10^9$ | 0.6690 | 1.0 | 0.497 | | |
| 27 | 10.346 | | | | | | |
| 28 | 3.449 | | | | | | |
| 29 | 6.897 | $3.57\times10^{15}$ | 0.6643 | 3.0 | 1.50 | | |
| 30 | 10.346 | | | | | | |
| 31 | 3.449 | | | | | | |

[a] Units: $[g^{1-m}cm^{m-1}s^{-1}K^{-\beta_g}]$, $m=\Phi_F+\Phi_O$

## Results and Discussion

### Physical Parameters

Values of the physical parameters held fixed in the present analysis are listed in Table 1. The flame temperature, propellant density, specific heats, and average (product) molecular weight are appropriate to JPN, according to Wimpress.[23] The viscosity relation is used in the analysis of Peretz et al.[24] The pyrolysis constants $A_\pi$, $\beta_\pi$, and $T_{A\pi}$ are believed typical of those used for propellant-stability studies, and yield a surface temperature $T_s = 725$ K when $\dot{r} = 1$ cm/s. The heat of decomposition at reference condition ($L_s^0$, 0 K) is considered to be exothermic by at least $-100$ cal/g for a monopropellant such as ammonium perchlorate.[25] However, an apparently intrinsic (nonnumerical) instability was noticed in some preliminary computations when $L_s^0$ was less than about $-50$ cal/g. The value of $-20$ was selected to ensure stability over a range of physical conditions.

Table 2 lists the parameters varied in the present study and the corresponding computer run numbers. For each of the thermodynamic or kinetic parameters varied, the normal (nonerosive, steady-state) burning rate was first obtained by solving the energy Eq. (20) alone, with $\bar{u} = \overline{u_i' u_j'} = 0$ and with the term $\bar{\rho}\bar{u}\bar{h}_{,x}$ replaced by $\bar{\rho}\bar{h}_{,t}$. It was found that the normal burning rate for all conditions in Table 2 could be represented by $\dot{r}_n/\dot{r}_* = (p/p_*)^n \pm 5\%$, over the range $0.5 \le p/p_* \le 2$. Table 2 also gives the values of $\dot{r}_*$ (normal burning rate at $p_* = 6.9 \times 10^7$ dyn/cm$^2$) and $n$.

### External Velocity Effect

Figure 2 shows the effect of constant boundary-layer edge velocity $U_e = U_e^0$ on propellant recession ratio $\dot{r}/\dot{r}_n$ as a function of distance $x$ along the propellant surface. There is a significant ($\approx 30\%$) reduction in burning rate over the first 10 cm of propellant. A similar decrease was noticed in the composite propellant experiments of Marklund and Lake.[26] Their apparatus produced an approximately constant "crossflow" velocity over a 7-cm-long propellant test strip. This downstream decrease in burning for constant edge velocity boundary layers has been shown to be caused by the rapid growth in viscous sublayer thickness.[15] Figure 2 also shows that the normal burning rate is recovered at $U_e = 200$ m/s for $x > 30$, and corresponds with the velocity boundary layer detaching from the propellant surface (i.e., exhibiting no surface skin friction). This "blowoff" behavior was discussed by Jeromin[27] and occurs in turbulent boundary layers with sufficiently large surface-to-edge mass-transfer ratios. Edge velocities less than 100 m/s were investigated, but for these values the boundary layer detached almost immediately. No evidence of "negative erosion"[1] was found in the low $U_e$ investigation.

### Channel-Width Effect

Figure 3 shows the results of varying the channel width $s$ to provide a propellant-induced velocity increase along the channel. The departure from a linear $x$ dependence of $U_e$ (solid lines) is due to the erosive burning effect. The severity of erosive burning for the narrower channel widths ($s = 0.5$, 0.7 cm) is shown. The value of $s = 0.7$ is approximately equal to the initial 0.64-cm width of the rectangular grain port of Peretz et al.[24] However, an obvious problem arises in the use of small channel widths while also using asymptotic boundary conditions for the dependent variables. The velocity boundary-layer thickness for run 9 ($s = 0.50$ cm) grows from its initial value of 0.179 cm to 0.937 cm at $x = 100$. Most of the growth occurs over the first 10 cm of propellant, with the growth rate diminishing rapidly as the velocity along the channel increases. Despite the large velocity boundary-layer thickness, the momentum and displacement thicknesses remain smaller than the channel half-width. It is therefore believed that the results obtained for the finite values of $s$ qualitatively reflect the conditions found in small port diameter motors.

### Comparison of Results for Constant Velocity and Accelerated Flows

Figure 4 shows the recession ratio as a function of boundary-layer-edge velocity, $U_e$. The propellant properties are identical for each of the velocity-response curves shown. The dashed lines are the constant $U_e$ calculations of Fig. 2. These may be considered to represent the recession-ratio results of a propellant tested with driver-flow apparatus. The solid lines are the varying $U_e$ calculations of Fig. 3, and simulate, for example, the results of interrupted burning experiments in two-dimensional grain ports. It is apparent that velocity alone is insufficient to scale the recession-ratio calculations, even at approximately constant static pressure. The calculations for constant $U_e$ are dependent on downstream position (as in the strip method of Marklund and Lake), while those for varying $U_e$ exhibit a channel-width effect. Both effects should be accounted for in predicting full-scale motor performance from erosive burning test data.

In the absence of convective flow, the present theory essentially reduces to the steady-state monopropellant deflagration theory of Johnson and Nachbar. Despite the monopropellant limitation, the erosive burning results of Fig. 4 are similar in shape to the experimental results obtained by Wimpress (for double-base propellants) and Marklund and Lake (for composite propellants). The present calculations for recession ratio as a function of external velocity do, however, fall below observed magnitudes by a factor of about two or three for low-burning-rate propellants. Figure 4 also displays

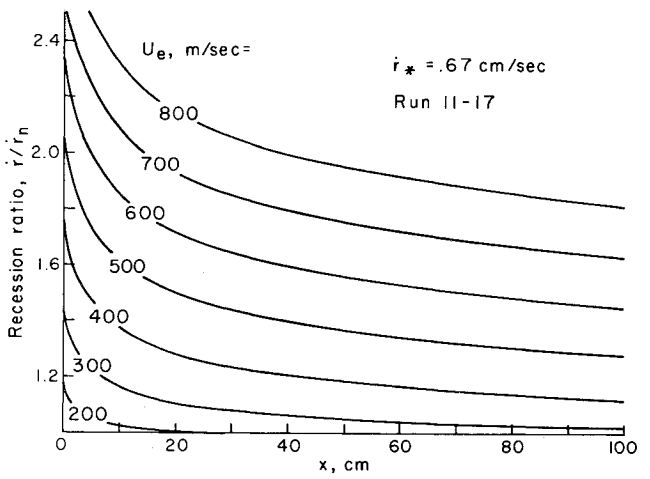


Fig. 2 The effect of constant boundary-layer-edge velocity $U_e$ on recession ratio $\dot{r}/\dot{r}_n$ as a function of distance along the propellant $x$.

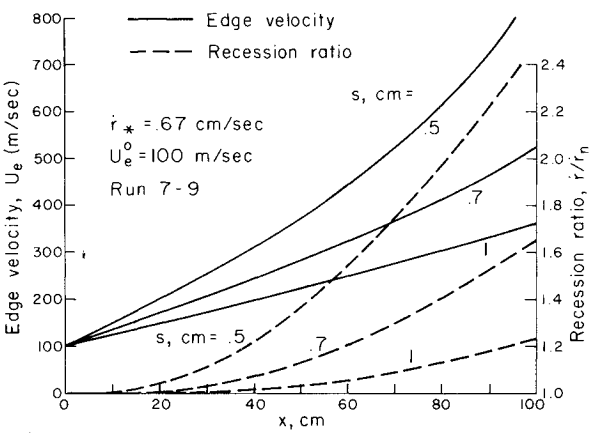


Fig. 3 The effect of channel width $s$ on boundary-layer edge velocity and recession ratio as a function of distance along the propellant $x$.

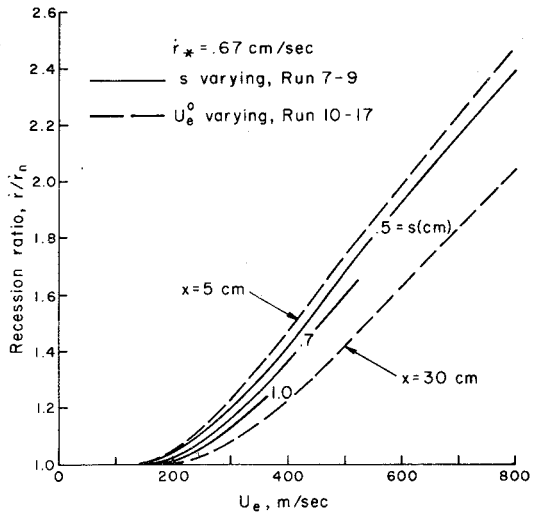


Fig. 4 Length scale effects on recession ratio as a function of boundary-layer edge velocity.

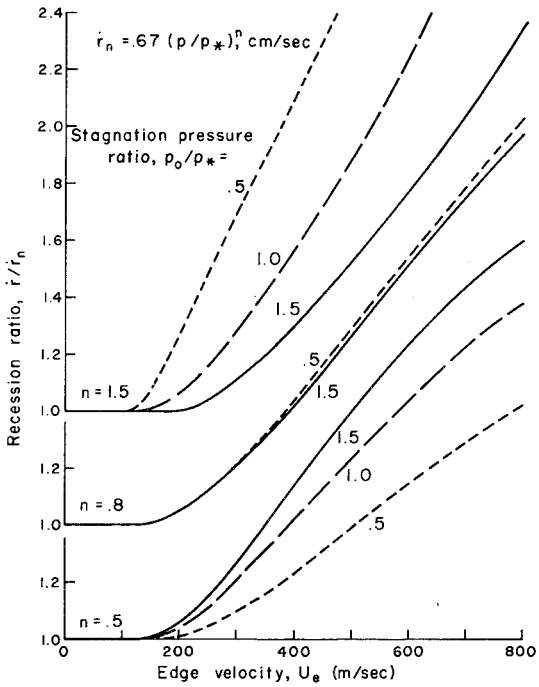


Fig. 5 The effects of stagnation pressure $p_0$ and normal burning-rate pressure exponents $n$ on recession ratio.

the generally observed phenomenon[1-3] of threshold velocity (velocity below which $\dot{r}/\dot{r}_n \leq 1$). Calculated boundary-layer profiles (to be discussed) show that threshold velocity is associated with sufficient turbulence entering the flame zone, as hypothesized by Corner.[4]

### Pressure Effect

Figure 5 shows the effect of a ±50% variation of stagnation pressure ($p_0$) on recession ratio, for three values of burning-rate pressure exponent $n$. The values of $n$ are obtained by altering the overall reaction order ($\Phi_F + \Phi_0$), while maintaining constant $\dot{r}_*$. For $n=0.8$, slight pressure dependence is observed. This is constant with the experimental observations of Wimpress for homogeneous propellants with similar values of pressure exponent. For $n=0.5$, a value which is more in line with composite propellants, a pronounced effect of pressure on recession ratio is seen in the calculations. The trend for this lower pressure exponent is such that for constant velocity,

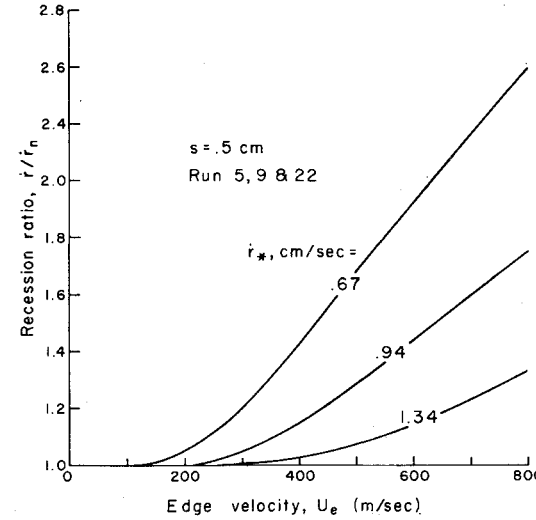


Fig. 6 The effect of normal burning rate on recession ratio.

propellant erosion increases with increasing stagnation pressure. Similar pressure trends have been experimentally observed, particularly for composite propellants.[1,2,26] Results for a pressure exponent of 1.5 show a reversal of the pressure trend, since the recession ratio decreases as $p_0$ increases. The calculations of Fig. 5 additionally indicate that as the pressure exponent decreases, the downward curvature of the recession ratio at higher velocities increases. This nonlinear behavior (i.e., $\dot{r}/\dot{r}_n \sim U_e^m$, $m<1$) is typical of experimental results.[2,23,26]

### Normal Burning-Rate Effect

It is well established[23,26,28] that higher burning-rate propellants exhibit less tendency toward erosion. This effect is shown by the calculation in Fig. 6. The reference normal burning rate $\dot{r}_*$ is altered by adjusting the reaction preexponential factor $B_g$. The slope of the velocity response above threshold $(\partial\dot{r}/\dot{r}_n/\partial U_e)$ is shown to diminish with increasing $\dot{r}_*$. This is consistent with the trend observed by Green[28] for composite and homogeneous propellants. It has also been generally observed[1,3] that the threshold velocity increases with normal burning rate—a trend with which the calculations agree.

### Boundary-Layer Profiles

Calculated boundary-layer profiles of mean and turbulent variables can provide information about suspected causes of erosive burning. Profiles of a constant external velocity boundary layer (characteristic of driver flow test apparatus) show a gradual withdrawal of turbulence from the propellant flame zone and consequent decrease of erosion.[15] Profiles of an accelerating boundary layer are more representative of grain-port conditions and are shown in Fig. 7. The mean temperature and longitudinal-velocity component, and the correlations $\overline{h'v'}$ and $\overline{u'v'}$, are provided for successive downstream distances $x$. Note that the quantities $\bar{\rho}\overline{h'v'}$ and $-\bar{\rho}\overline{u'v'}$ are the turbulent fluxes (to second-order) of heat and momentum within the boundary layer.

In the initial region of flow, the temperature profile (Fig. 7a, $x=1$ cm) is virtually identical to that obtained for normal burning. However, the velocity-proile gradient increases in the downstream boundary layer and produces a corresponding increase in the turbulent shear-stress correlation, $\overline{u'v'}$. The larger amounts of turbulence now entering the flame zone increase the magnitude of the turbulent heat-transfer correlation $\overline{h'v'}$ and move the location of minimum $\overline{h'v'}$ inward. This process apparently causes erosive burning to commence, as is noted from the results of run 9 in Fig. 3. The effect of significant $\overline{h'v'}$ is to broaden the temperature profile in the flame zone, as seen in the profiles at $x=50$ and 75. The

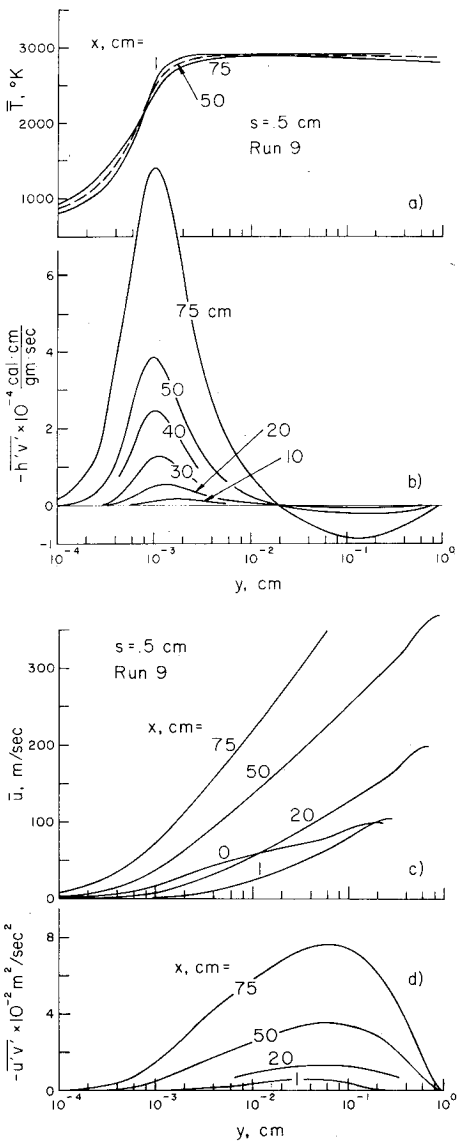


**Fig. 7 Boundary-layer profiles in a channel-flow simulation: a) mean temperature; b) heat-transfer correlation; c) mean velocity; d) shear-stress correlation.**

phenomenon of flame-zone broadening is associated with small-scale-turbulence effects on homogeneous premixed flames.[12] Comparison of the temperature profile at $x=75$ with the results of Fig. 3 shows that the observed increase in temperature gradient provides an 85% increase in recession rate.

## Summary

Solid propellant erosive burning has been investigated using a reacting turbulent boundary approach. The important details of turbulence development are obtained with the second-order closure technique, and a single-step global reaction is assumed for the combustion of a homogeneous propellant. Use of this combustion model (i.e., the monopropellant model of Johnson and Nachbar) represents an idealization of the combustion mechanism of practical propellants. The present analysis is therefore restricted to the consideration of erosive burning trends that have been observed for most propellant types.

The theoretical methods is found to be in agreement with the generally observed trends of threshold velocity, nonlinear recession-ratio velocity dependence, pressure dependence, and normal burning-rate sensitivity. The theory displays the transient erosive burning effect noted in the experiments of Marklund and Lake,[26] and also exhibits a dependence on channel width (through pressure gradient) in simulations of grain-port flow. A more accurate analysis of grain-port flow is necessary to verify the latter observation.

The ability of the theory to provide boundary-layer profiles of the mean and turbulent fields has been utilized to investigate the cause of erosive burning for the assumed combustion mechanism. Consistent with the concept of Corner[4] and others, erosive burning appears coincidentally with turbulence entering the flame zone. The mechanism of increased surface heat transfer is associated with flame-zone broadening due to the diffusive effects of turbulence. The profile results also indicate that underprediction of erosion data by the present model may, in part, be caused by the rather low flame standoff distances produced by the combustion mechanism.

## References

[1] Williams, F. A., Barrere, M., and Huang, N. C., "Fundamental Aspects of Solid Rockets," AGARDograph 116, Chapts. 4, 6, and 7, Oct. 1969, pp. 339-456.

[2] King, M. K., "A Model of Erosive Burning of Composite Propellants," Paper 77-930, AIAA/SAE 13th Propulsion Conference, July 1977; also, *Journal of Spacecraft and Rockets*, Vol. 15, May-June 1978, pp. 139-146.

[3] Kuo, K. K. and Razdan, M. K., "Review of Erosive Burning of Solid Propellants," *Proceedings of the 12th JANNAF Combustion Meeting*, Aug. 1975, pp. 323-338.

[4] Corner, J., "The Effects of Turbulence on Heterogeneous Reaction Rates," *Transactions of the Faraday Society*, Vol. 43, 1947, pp. 635-642.

[5] Vandenkerckhove, J. A., "Erosive Burning of a Colloidal Solid Propellant," *Jet Propulsion*, Vol. 28, Sept. 1958, pp. 599-603.

[6] Lengellé, G., "Model Describing the Erosive Combustion and Velocity Response of Composite Propellants," *AIAA Journal*, Vol. 13, Mar. 1975, pp. 315-322.

[7] Lenoir, J. M. and Robillard, G., "A Mathematical Method to Predict the Effects of Erosive Burning in Solid Propellant Rockets," *Proceedings of the 6th Symposium (International) on Combustion*, Reinhold, New York, 1957, pp. 663-667.

[8] Tsuji, H., "An Aerothermochemical Analysis of Erosive Burning of Solid Propellants," *Proceedings of the 9th Interntional Symposium on Combustion*, Williams & Wilkins, Baltimore, Md., 1963, pp. 384-393.

[9] Schuyler, F. L. and Torda, T. P., "An Aerothermochemical Analysis of Solid Propellant Combustion," *AIAA Journal*, Vol. 4, Dec. 1966, pp. 2171-2177.

[10] Varma, A. K., Beddini, R. A., Sullivan, R. D., and Donaldson, C. duP., "Application of an Invariant Second-Order Closure Model to the Calculation of Compressible Boundary Layers," AIAA Paper 74-592, 7th Fluid and Plasma Dynamics Conference, June 1974.

[11] Razdan, M. K. and Kuo, K. K., "Erosive Burning Studies of Composite Propellants by the Reacting Turbulent Boundary-Layer Approach," Interim Rept., Pennsylvania State University, University Park, Pa., Nov. 1976.

[12] Williams, F. A., *Combustion Theory*, Addison-Wesley, Reading, Mass., 1965, Chapts. 1, 5, and 7.

[13] Johnson, W. E. and Nachbar, W., "Deflagration Limits in the Steady Linear Burning of a Monopropellant with Application of Ammonium Perchlorate," *Proceedings of the 8th International Symposium on Combustion*, Williams & Wilkins, Baltimore, Md., 1962, pp. 678-689.

[14] Glasstone, S., *Textbook of Physical Chemistry*, 2nd Ed., Van Nostrand, Princeton, N.J., 1946, pp. 453-460.

[15] Beddini, R. A., "A Reacting Turbulent Boundary Layer Approach to Solid Propellant Erosive Burning," AFOSR-TR-77-1310, Nov. 1977; also Beddini, R. A. and Fishburne, E. S., "Analysis of the Combustion-Turbulence Interaction Effects on Solid Propellant Erosive Burning," Paper 77-931, Orlando, Fla., July 1977.

[16] Hinze, J. O., *Turbulence*, 2nd Ed., McGraw-Hill, New York, 1975, Chapts. 5 and 7.

[17] Yamada, K., Goto, M., and Ishikawa, N., "Simulative Study on the Erosive Burning of Solid Rocket Motors," *AIAA Journal*, Vol. 14, Sept. 1976, pp. 1170-1177.

[18] Varma, A. K., Fishburne, E. S., and Donaldson, C.duP., "Aspects of Turbulent Combustion," AIAA Paper 77-100, 15th Aerospace Sciences Meeting, Jan. 1977.

[19] Rubesin, M. W., Crisalli, A. J., Lanfranco, M. J., Horstman, C. C., and Acharya, M., "A Critical Evaluation of Second-Order Closure Models for Incompressible and Compressible Boundary Layers with Axial Pressure Gradient," AIAA Paper 77-128, 15th Aerospace Sciences Meeting, Jan. 1977.

[20] Sullivan, R. D., "GYC—A Program to Compute the Turbulent Boundary Layer on a Rotating Cone," Aeronautical Research Associates of Princeton, Inc., Working Paper 76-2, Aug. 1976.

[21] Dunlap, R., Willoughby, P. G., and Hermsen, R. W., "Flowfield in the Combustion Chamber of a Solid Propellant Rocket Motor," *AIAA Journal*, Vol. 12, Oct. 1974, pp. 1440-1442.

[22] Vilyunov, V. N. and Dvoryashin, A. A., "An Experimental Investigation of the Erosive Burning Effect," *Combustion, Explosion and Shockwaves* (USSR), 1973, pp. 38-42.

[23] Wimpress, R. N., *Internal Ballistics of Solid Fuel Rockets*, McGraw-Hill, New York, 1950, Chapts. 2 and 6.

[24] Peretz, A., Kuo, K. K., Caveny, L. H., and Summerfield, M., "Starting Transient of Solid-Propellant Rocket Motors with High Internal Gas Velocities," *AIAA Journal*, Vol. 11, Dec. 1973, pp. 1719-1727.

[25] Guirao, C. and Williams, F. A., "A Model for Ammonium Perchlorate Deflagration Between 20 and 100 Atm," *AIAA Journal*, Vol. 9, July 1971, pp. 1345-1356.

[26] Marklund, T. and Lake, A., "Experimental Investigation of Propellant Erosion," *ARS Journal*, Vol. 30, Feb. 1960, pp. 173-178.

[27] Jeromin, L. O. F., "An Experimental Investigation of the Compressible Turbulent Boundary Layer with Air Injection," Aeronautical Research Council, R&M 3526, 1968.

[28] Green, L., "Erosive Burning of Some Composite Solid Propellants," *Jet Propulsion*, Vol. 24, Jan.-Feb. 1954, pp. 9-15.